*Desalination and Water Treatment*
www.deswater.com

doi: 10.5004/dwt.2019.23472

140 (2019) 283–289
February

# Preparation of silver-doped $BiFeO_3$-MWCNT nanocomposites as enhanced photocatalysts for industrial wastewater remediation

Reda M. Mohamed[a,b,*], Mohammad W. Kadi[a]

[a]*Department of Chemistry, Faculty of Science, King Abdulaziz University, P.O. Box 80203, Jeddah 21589, Kingdom of Saudi Arabia, Tel. +966 540715648; Fax: +966 2 6952292; emails: redama123@yahoo.com (R.M. Mohamed), mkadi10@gmail.com (M.W. Kadi)*
[b]*Advanced Materials Department, Central Metallurgical R&D Institute, CMRDI, P.O. Box 87, Helwan, Cairo 11421, Egypt*

Received 14 July 2018; Accepted 16 November 2018

**ABSTRACT**

$BiFeO_3$ nanoparticles, Ag/$BiFeO_3$ nanoparticles, and Ag/$BiFeO_3$-MWCNTs (multiwall-carbon nanotubes) nanocomposites were successfully prepared by simple routes and investigated using different tools to explore and reveal their chemical and physical properties. transmission electron microscopy showed that $BiFeO_3$ nanoparticles and Ag/$BiFeO_3$ nanoparticles were homogenously distributed on the tangled MWCNT surface. Furthermore, the addition of silver and MWCNTs to $BiFeO_3$ nanoparticles greatly reduced the band gap of $BiFeO_3$ nanoparticles and enhanced their efficiency for cyanide degradation under visible light irradiation. Finally, Ag/$BiFeO_3$-MWCNTs nanocomposites showed great photocatalytic stability for cyanide degradation in an aqueous solution over five cycles of reuse.

*Keywords:* Cyanide; Ag; MWCNTs; Photocatalyst; Visible light; $BiFeO_3$

## 1. Introduction

Aquatic pollution by cyanide is mainly due to different anthropogenic activities, such as pharmaceutical industry activities, metal extraction, photography, metal finishing, steel tempering, electroplating, coal processing and automobile parts manufacturing [1]. Mainly because of its high toxicity, cyanide threatens the lives of flora and fauna. [2]. Cyanide can be found in organic and inorganic forms and is characterized by its very low median lethal dosage in mammals, which ranges from 1.3 to 10 mg/kg body weight [3]. Currently, there are many procedures that can be used to eliminate cyanide from polluted water, such as biodegradation using fungi, bacteria, and algae [4]; adsorption using solid adsorbents [5,6]; coagulation [7]; precipitation [8]; Fenton oxidation [9]; hydrogen per oxide oxidation [10]; plasma discharge technology [11]; and photocatalytic degradation [12–14]. Currently, photocatalytic removal of pollutants from industrial wastewater has led to fruitful and economic benefits for both industry and the environment. The photocatalytic process usually occurs via absorption of incident light on a semiconductor. Photocatalytic degradation using semiconductors is considered to be the most promising procedure for environmental remediation of pollutants such as cyanide due to its ease of application, low cost, and reliability. $TiO_2$ nanoparticles have high photocatalytic activity in the UV region and have been used extensively for the degradation of many pollutants in aqueous solution, including cyanide [15,16]. The $TiO_2$ photocatalyst is characterized by its low cost, high chemical stability, outstanding photocatalytic activity, and nontoxic nature [17]; however, it has many disadvantages, such as a broad band gap energy (3.2 eV), prevent its application using visible light as well as its high electron–hole recombination rate [18]. Doping and modification of $TiO_2$ photocatalysts with other materials are other solutions for such problems [19–22]. $BiFeO_3$ is another photocatalyst that has been used for photocatalytic degradation of many pollutants in water [23–29] due to its low toxicity and small size. However, some limitations

* Corresponding author.

have been noted in regard to its photocatalytic efficiency due to its large recombination and small surface area. Recently, many studies have shown the increased photodegradation efficiency of $BiFeO_3$ through several procedures, including boosting the surface-to-volume ratio of the catalyst and doping transition metals, non-metals, and precious metals onto the surface of $BiFeO_3$ [30–47]. Recently, metal doped-$BiFeO_3$ nanocomposites have attracted significant interest due to the extensive spectrum of their potential applications. The presence of unique surface chemical species on the surface of metal doped-$BiFeO_3$ heterostructures has been investigated, and its photocatalytic efficiency for the degradation of 4-chlorophenol over visible light illumination has been studied [34]. Metal doped-$BiFeO_3$ materials have various surface characteristics that might be able to be employed for designing new devices with developed properties [35]. Metal doped-$BiFeO_3$ exhibits outstanding photocatalytic efficiency under visible light to degrade rhodamine B [36]. Doping of $BiFeO_3$ with transition metals signifies one solution to reduce the high recombination rate by inducing an intermediate state. In addition, forming nanocomposites by hybridization or coupling with other materials showed that a large surface area and electron mobility are significant strategies to produce an efficient photocatalyst. Multiwall-carbon nanotubes (MWCNTs) are powerful materials that can be coupled with the $BiFeO_3$ photocatalyst due to its incredible and unique properties. The use of carbon nanotubes (CNTs) in photocatalysis began directly after its discovery in 1991 by Iijima [48]. CNTs are important materials among carbon allotropes. CNTs have a unique structure that is due to rolling a graphene sheet into cylindrical shape. CNTs can be single-walled carbon nanotubes (SWCNTs) or multi-walled (MWCNTs). Due to the electronic structure, high surface area, and adsorptive chemical stability of CNTs, they have been used in photocatalytic applications [49–52]. Thus, the use of MWCNTs with $BiFeO_3$ nanoparticles is expected to enhance the photocatalytic activity of $BiFeO_3$. In a photocatalytic manner, MWCNTs can adjust the $BiFeO_3$ band structure by generating a defect structure that enhances its hole and electron redox energy potential. On the other hand, MWCNTs can successfully hinder the recombination of the photogenerated electrons and its hole, thereby enhancing the photocatalytic properties [53]. Therefore, as a green, effective and non-toxic strategy for wastewater remediation, silver doped-$BiFeO_3$ nanostructure-supported MWCNTs were prepared to form materials with high activity for the degradation of toxic organic materials in industrial wastewater. The nanocomposites were prepared under mild conditions by a simple sol-gel process with an expected good yield and enhanced the removal of toxic materials from water. In this regard, this project is expected to achieve excellent remediation of industrial wastewater that can save the environment and economy.

## 2. Experimental setup

### 2.1. Materials

All reagents were used as-received and were of analytical grade. $Bi(NO_3)_3{\cdot}5H_2O$, $Fe(NO_3)_3{\cdot}9H_2O$, potassium hydroxide, silver nitrate, MWCNTs, ethanol absolute were purchased from Sigma-Aldrich and were used as-received.

### 2.2. Preparation of materials

#### 2.2.1. $BiFeO_3$ nanoparticles preparation

$BiFeO_3$ nanoparticles were prepared by the hydrothermal method according to the following: $Bi(NO_3)_3.5H_2O$ (16 mmol), potassium hydroxide (100 mmol) and $Fe(NO_3)_3.9H_2O$ (8 mmol) were dissolved in deionized $H_2O$ (60 mL), and the resulting blend was stirred at ambient temperature for 60 min. Then, the blend was heated in a 100 mL Teflon-lined stainless autoclave for 24 h at 403 K. After the autoclave cooled, the produced materials were washed a number of times with deionized $H_2O$ and ethanol and dried under a vacuum for 8 h at 333 K.

#### 2.2.2. Ag/$BiFeO_3$ nanoparticle (2 wt%) preparation

Ag/$BiFeO_3$ nanoparticles (2 wt%) were prepared by photo-assisted deposition according to the following: 0.06 g of silver nitrate was dissolved in 100 mL of deionized water. Two grams of $BiFeO_3$ nanoparticles was dispersed into an aqueous solution of silver nitrate, and the obtained blend was exposed to a xenon lamp at 500 W for 24 h at room temperature. Ag/$BiFeO_3$ nanoparticles (2 wt%) were collected by filtration and washed a number of times with water and ethanol; the sample was finally dried for 24 h at 353 K.

#### 2.2.3. $BiFeO_3$-MWCNT-4 wt% nanocomposite preparation

MWCNT (0.08 g) was dissolved in 100 mL ethanol via sonication for 2 h. Then, 2 g of the prepared $BiFeO_3$ nanoparticles was discrete in 20 mL deionized water via sonication for 30 min. Finally, the dissolved MWCNT was added to dissolved $BiFeO_3$ nanoparticles, and the mixture was refluxed for 6 h. $BiFeO_3$-MWCNT-4 wt% nanocomposites were collected by filtration and washing a number of times with water and ethanol; the sample was finally dried for 24 h at 373 K.

#### 2.2.4. Preparation of 2 wt% Ag/BiFeO3-MWCNT-4 wt% nanocomposites

$BiFeO_3$-MWCNT-4 wt% nanocomposites were prepared by the photo-assisted deposition method according to the following: 0.06 g of silver nitrate was dissolved in 100 mL of deionized water. $BiFeO_3$-MWCNT-4 wt% nanocomposites (2 g) were dispersed into an aqueous solution of silver nitrate, and the obtained blend was exposed to a xenon lamp (500 W) for 24 h at room temperature. Ag/$BiFeO_3$-MWCNT-4 wt% nanocomposites (2 wt%) were collected by filtration and washed a number of times with water and ethanol; the sample was then dried for 24 h at 353 K.

### 2.3. Characterization techniques

The physical, chemical and morphological properties of $BiFeO_3$ nanoparticles, Ag/$BiFeO_3$ nanoparticles, and Ag/$BiFeO_3$-MWCNTs nanocomposites were investigated using different characterization techniques. The nanostructure morphology and sample dimensions were investigated using transmission electron microscopy (TEM), JEM-1230 (JEOL). Surface area analysis was performed and the textural properties were investigated using a Nova 2000 series

Chromatech apparatus at 373 K. The crystallinity of the samples was investigated using a powder X-ray diffraction (XRD) AXS D8 (Bruker) with Cu Kα radiation (λ = 1.540 Å) at room temperature. The photoluminescence (PL) emission spectra were investigated using a RF-5301 fluorescence spectrophotometer (Shimadzu). The UV-Vis diffuse reflectance spectra (UV-Vis-DRS) were investigated using a UV-Vis-NIR spectrophotometer, V-570, JASCO, Japan.

### 2.4. Photocatalytic activity

The photocatalytic activities of $BiFeO_3$ nanoparticles, Ag/$BiFeO_3$ nanoparticles, and Ag/$BiFeO_3$-MWCNTs nanocomposites were explored for cyanide degradation under visible light irradiation in a horizontal cylinder annular batch reactor according to the following steps: (1) a blue fluorescent lamp (150 W) was applied for irradiation of the photocatalyst, and a UV cut filter was applied to remove UV light below 420 nm; (2) $BiFeO_3$ nanoparticles, Ag/$BiFeO_3$ nanoparticles or Ag/$BiFeO_3$-MWCNTs nanocomposites were suspended in a 300 mL volume and 100 ppm concentration potassium cyanide solution; (3) to avoid evolution of HCN gas, an ammonia solution was used to adjust the pH to 10.5; (4) the reaction temperature was adjusted to 298 K, and the total reaction time was 60 min; and (5) volumetric titration with $AgNO_3$ was used to measure the cyanide concentration after photocatalysis using potassium iodide as an indicator.

The following equation was used to calculate the cyanide removal efficiency, %:

$$\text{Cyanide removal efficiency, \%} = (C_o - C)/C_o \times 100$$

where $C_o$ is the cyanide initial concentration in the solution; $C$ is the remaining cyanide concentration in the solution.

## 3. Results and discussion

### 3.1. Photocatalysts characterizations

Fig. 1 shows the XRD patterns for the MWCNT, $BiFeO_3$, 2 wt% Ag/$BiFeO_3$, and 2 wt% Ag/$BiFeO_3$-MWCNT-4 wt% samples. Regarding the $BiFeO_3$ diffraction pattern, the results reveal the presence of a rhombohedral phase for $BiFeO_3$ (JCPDS 71-2494). Regarding the Ag/$BiFeO_3$ nanoparticles sample, the characteristic diffraction peaks of a rhombohedral phase for $BiFeO_3$ (JCPDS No. 71-2494) were observed, and there were no peaks for silver or silver oxide due to the high distribution of silver on the surface of $BiFeO_3$, as seen in the TEM images or by low weight percent of decorated silver. Regarding the MWCNTs sample, the characteristic diffraction peak of MWCNTs at approximately 23.0° corresponding to the diffraction peak of (002) of MWCNTs (JCPDS card no. 26-1079) was present. Regarding the Ag/$BiFeO_3$-MWCNTs sample, the characteristic diffraction peaks of $BiFeO_3$ were present, and no peaks for silver or MWCNT were found due to the high distribution of MWCNT and silver.

Fig. 2 shows TEM images of $BiFeO_3$ nanoparticles (a), Ag/$BiFeO_3$ (b), MWCNTs (c) and Ag/$BiFeO_3$-MWCNTs nanocomposites (d), and the results reveal the irregular shapes of $BiFeO_3$ and the irregular distribution of silver on the $BiFeO_3$ surface, which had an average particle size of 20 and 3 nm, as shown in Figs. 2(a) and (b), respectively. MWCNTs were long and entangled, with an average diameter of 20 nm, as is shown in the TEM image of Ag/$BiFeO_3$-MWCNTs nanocomposite in Fig. 2(c); Fig. 2(d) shows the dispersion of $BiFeO_3$ and silver nanoparticles on the surface of MWCNTs.

Table 1 provides the results of the surface area analysis of the MWCNT, $BiFeO_3$, 2 wt% Ag/$BiFeO_3$, and 2 wt% Ag/$BiFeO_3$-MWCNT-4 wt% samples. The outcomes illustrated that the surface areas were 165, 60, 50, and 100 $m^2/g$, for the MWCNTs, $BiFeO_3$, 2 wt% Ag/$BiFeO_3$, and 2 wt% Ag/$BiFeO_3$-MWCNT-4 wt% samples, respectively. Accordingly, it is clear that the addition of Ag and MWCNTs to $BiFeO_3$ significantly increased their BET surface area from 60 to 100 $m^2/g$ as a result of the distribution of silver and $BiFeO_3$ on the MWCNTs surface, similar to the TEM results.

The UV-Vis spectra of the MWCNT, $BiFeO_3$, 2 wt% Ag/$BiFeO_3$, and 2 wt% Ag/$BiFeO_3$-MWCNT-4 wt% samples were found and are presented in Fig. 3, and the results showed that absorption edges of $BiFeO_3$, 2 wt% Ag/$BiFeO_3$, and 2 wt% Ag/$BiFeO_3$-MWCNT-4 wt% samples were 516.6, 579.4, and 652.6 nm, respectively. Therefore, the $BiFeO_3$, 2 wt% Ag/$BiFeO_3$, and 2 wt% Ag/$BiFeO_3$-MWCNT-4 wt% samples absorb in the visible region. The band gap energy values of the $BiFeO_3$, 2 wt% Ag/$BiFeO_3$, and 2 wt% Ag/$BiFeO_3$-MWCNT-4 wt% samples were 2.40, 2.14, and 1.90 eV, respectively.

The PL spectra for $BiFeO_3$, 2 wt% Ag/$BiFeO_3$, and 2 wt% Ag/$BiFeO_3$-MWCNT-4 wt% samples were measured and are presented in Fig. 4. The results showed that the peak intensity of the PL spectra of the $BiFeO_3$, 2 wt% Ag/$BiFeO_3$, and 2 wt% Ag/$BiFeO_3$-MWCNT-4 wt% samples was decreased in the following sequence: $BiFeO_3$ > 2 wt% Ag/$BiFeO_3$ > 2 wt% Ag/$BiFeO_3$-MWCNT-4 wt%. The band gap energy of the $BiFeO_3$, 2 wt% Ag/$BiFeO_3$, and 2 wt% Ag/$BiFeO_3$-MWCNT-4

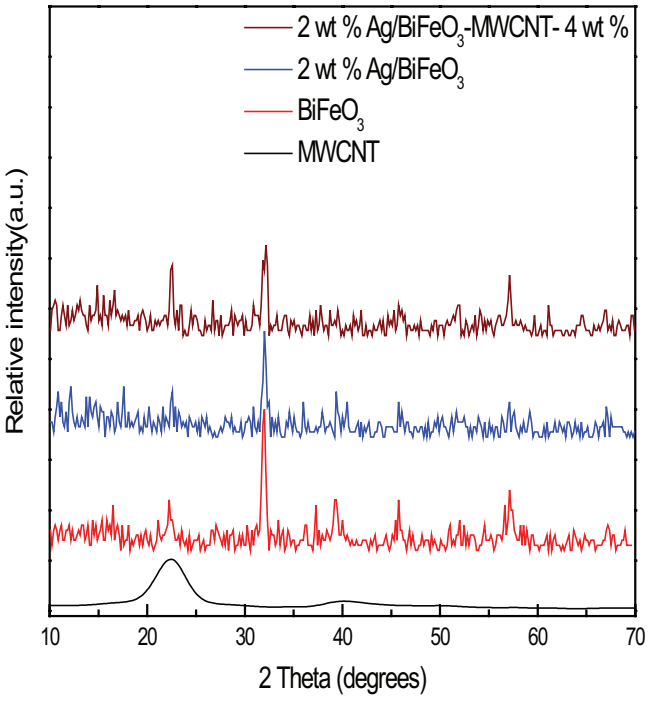


Fig 1. XRD patterns of the MWCNT, $BiFeO_3$, Ag/$BiFeO_3$, and Ag/$BiFeO_3$-MWCNT samples.

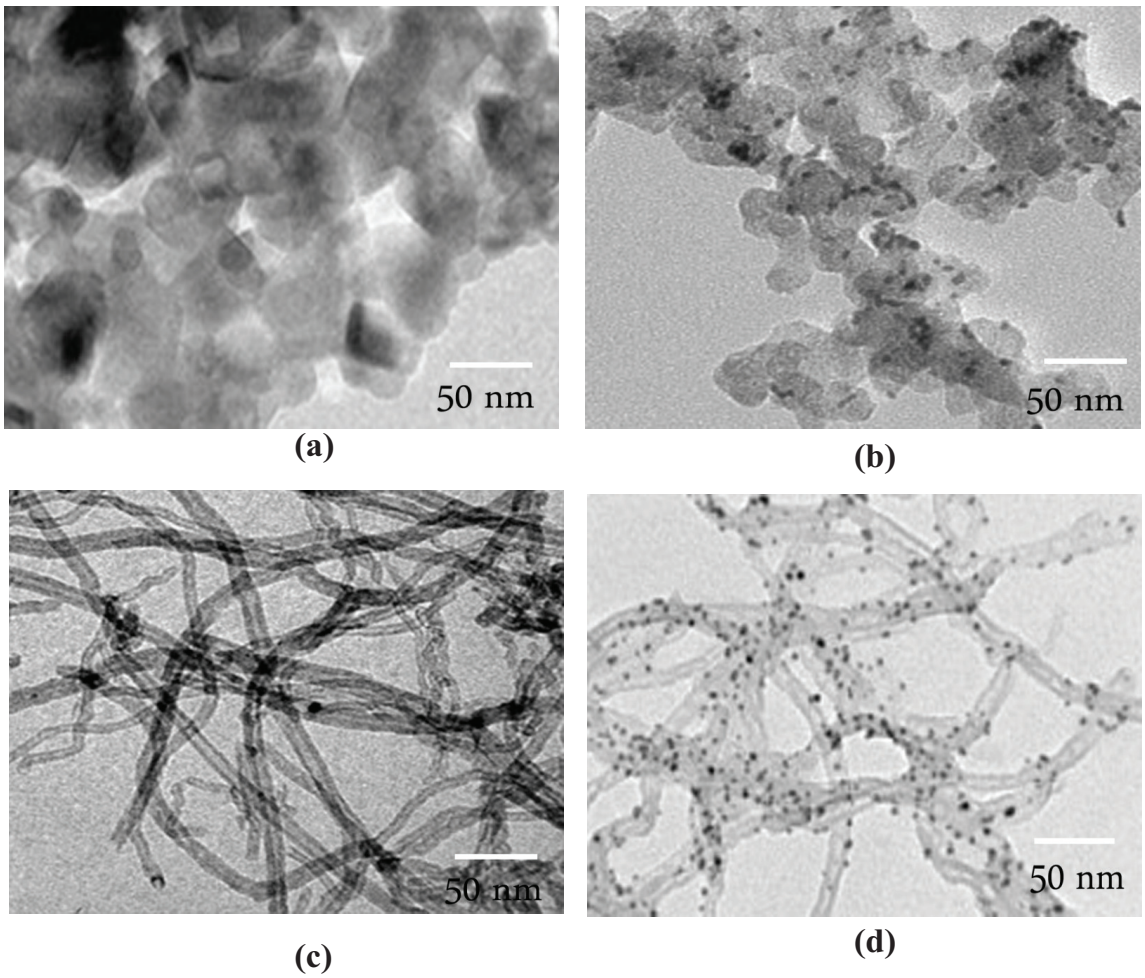


Fig. 2. TEM images of the $BiFeO_3$ (a), Ag-$BiFeO_3$ (b), MWCNT (c), and Ag/$BiFeO_3$-MWCNT nanocomposite (d) samples.

Table 1
Texture parameters of the MWCNT, $BiFeO_3$, 2 wt% Ag/$BiFeO_3$, and 2 wt% Ag/$BiFeO_3$-MWCNT-4 wt% samples

| Sample | $S_{BET}$ ($m^2/g$) | $S_t$ ($m^2/g$) | $S_{micro}$ ($cm^2/g$) | $S_{ext}$ ($cm^2/g$) | $V_p$ ($cm^3/g$) | $V_{micro}$ ($cm^3/g$) | $V_{meso}$ ($cm^3/g$) | $r$ (Å) |
|---|---|---|---|---|---|---|---|---|
| MWCNT | 165 | 166 | 63 | 102 | 0.900 | 0.100 | 0.800 | 35.00 |
| $BiFeO_3$ | 60 | 61 | 10 | 50 | 0.500 | 0.050 | 0.450 | 40.00 |
| 2 wt% Ag/$BiFeO_3$ | 55 | 56 | 8 | 47 | 0.440 | 0.040 | 0.400 | 45.00 |
| 2 wt% Ag/$BiFeO_3$-MWCNT-4 wt% | 100 | 102 | 5 | 95 | 0.790 | 0.090 | 0.700 | 30.00 |

$S_{BET}$, BET-surface area, $S_t$, surface area derived from $V_{l-t}$ plots, $S_{mic}$, surface area of micropores, $S_{ext}$, external surface area, $V_p$, total pore, $V_{mic}$, pore of micropores, $V_{mes}$, pore of mesopores, $r$, mean pore radius.

wt% samples, which had PL emission spectra of 2.19, 2.13, and 1.89 eV, respectively, were in excellent agreement with the values estimated from the UV-Vis spectra.

### 3.2. Photocatalytic performance

The performances of the MWCNT, $BiFeO_3$, 2 wt% Ag/$BiFeO_3$, and 2 wt% Ag/$BiFeO_3$-MWCNT-4 wt% samples for cyanide degradation under visible light were studied. Fig. 5 shows the photocatalytic degradation by the MWCNT, $BiFeO_3$, 2 wt% Ag/$BiFeO_3$, and 2 wt% Ag/$BiFeO_3$-MWCNT-4 wt% samples, and the outcomes indicate that the MWCNT sample alone has relatively no photocatalytic activity. Upon loading Ag with $BiFeO_3$ on MWCNT, the photocatalytic performance was increased from 0.4% to 100% due to the drastic reduction in the $BiFeO_3$ band gap from 2.40 to 1.90 eV due to the addition of Ag and MWCNT, which enables $BiFeO_3$ to absorb visible light as well as reduce the electron–hole recombination rate, as seen in the PL results.

Additionally, the effect of the dosage of the 2 wt% Ag/$BiFeO_3$-MWCNT-4 wt% sample on cyanide degradation was studied. Fig. 6 shows the effect of the dosage of the 2 wt%

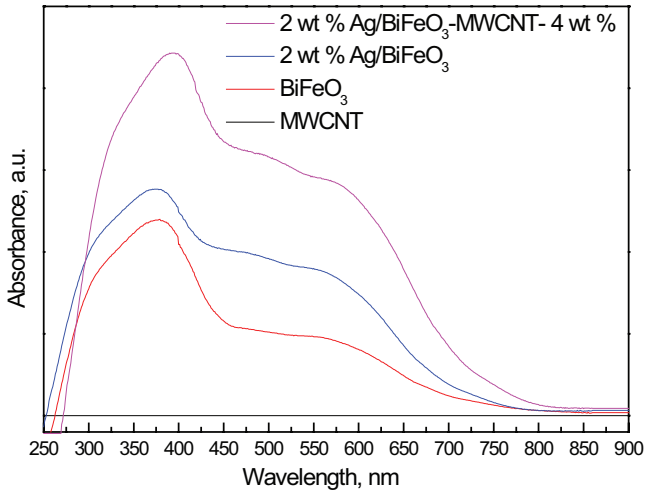


Fig. 3. UV-Vis spectra of the MWCNT, $BiFeO_3$, $Ag/BiFeO_3$, and $Ag/BiFeO_3$-MWCNT samples.

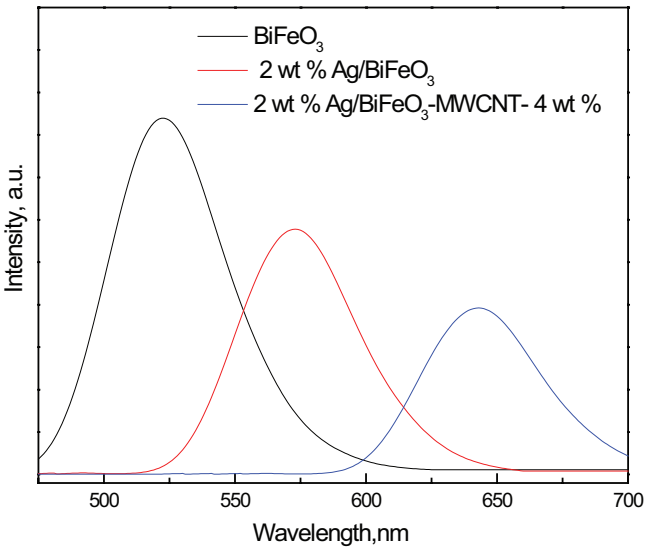


Fig. 4. PL spectra of the $BiFeO_3$, $Ag/BiFeO_3$, and $Ag/BiFeO_3$-MWCNT samples.

$Ag/BiFeO_3$-MWCNT-4 wt% sample on photocatalytic cyanide degradation, and the results indicate that the photocatalytic performance of 2 wt% $Ag/BiFeO_3$-MWCNT-4 wt% for cyanide degradation was increased from 70% to 100% by increasing the dosage of the 2 wt% $Ag/BiFeO_3$-MWCNT-4 wt% photocatalyst from 0.4 to 0.8 g/L because increasing the photocatalyst dosage usually raises the number of active sites that are accessible to the photocatalytic reaction and increases the photocatalytic performance. Additionally, increasing the dosage of the 2 wt% $Ag/BiFeO_3$-MWCNT-4 wt% nanocomposite photocatalyst from 0.8 to 1.6 g/L led to a reduction of the time required to achieve 100% cyanide degradation from 60 to 30 min. Additionally, the dosage of the 2 wt% $Ag/BiFeO_3$-MWCNT-4 wt% nanocomposite photocatalyst was increased to greater than 1.6 g/L, which led to an increase in the time required to achieve complete cyanide degradation from 30 to 40 min, which could be explained by the delay of

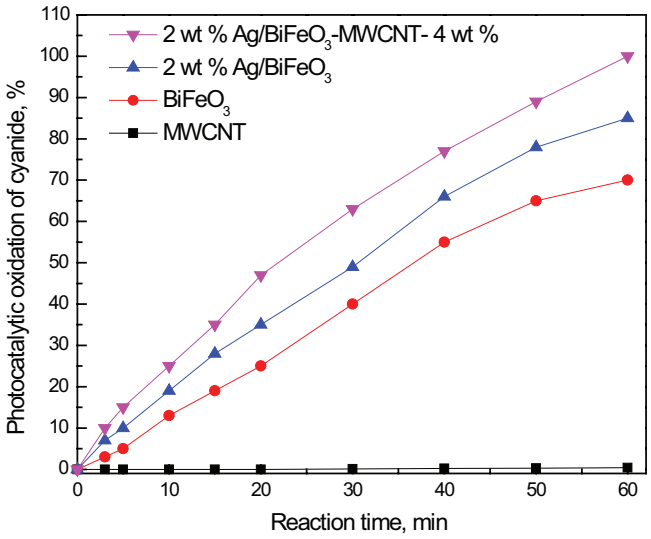


Fig. 5. Photocatalytic degradation of cyanide by the MWCNT, $BiFeO_3$, $Ag/BiFeO_3$, and $Ag/BiFeO_3$-MWCNT samples (experimental conditions: light source, 150 W blue fluorescent lamp; reaction time, 60 min, dosage of photocatalyst 0.8 g/L; volume of aqueous solution, 100 mL; and cyanide concentration, 100 mg/L).

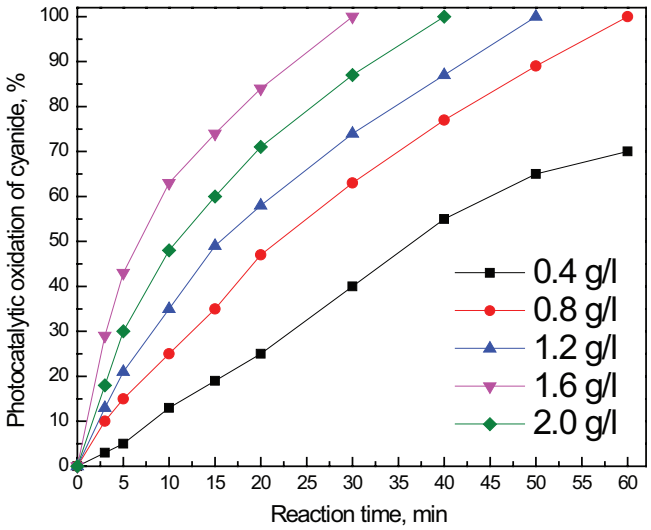


Fig. 6. Effect of the dosage of the $Ag/BiFeO_3$-MWCNT nanocomposite on the photocatalytic degradation of cyanide (experimental conditions: light source, 150 W blue fluorescent lamp reaction time, 60 min; dosage of photocatalyst, from 0.4 to 2.0 g/L; volume of aqueous solution, 100 mL; and cyanide concentration, 100 mg/L).

light arrival at the photocatalyst surface due to the high dosage of the 2 wt% $Ag/BiFeO_3$-MWCNT-4 wt% nanocomposite photocatalyst, which led to decreased photocatalytic activity.

Finally, the recycling and reuse of the 2 wt% $Ag/BiFeO_3$-MWCNT-4 wt% nanocomposite on cyanide degradation were explored, and the results are presented in Fig. 7. The results illustrated that the 2 wt% $Ag/BiFeO_3$-MWCNT-4 wt% nanocomposite photocatalyst has high stability and can be recycled several times without losing its efficiency.

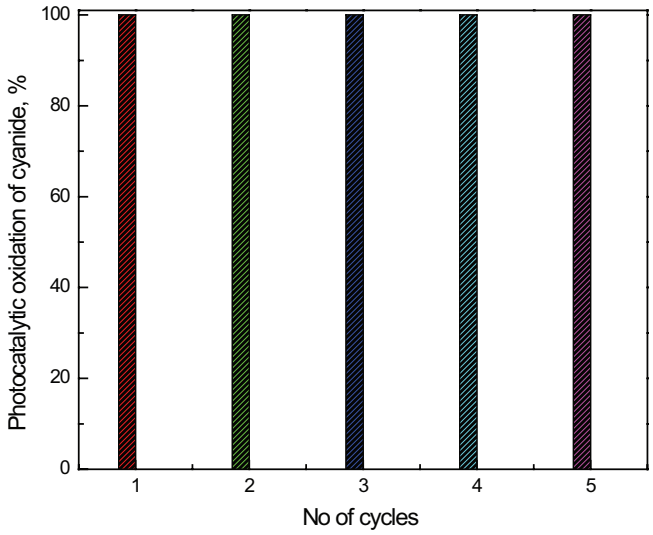


Fig. 7. Recycle and reuse of the Ag/$BiFeO_3$-MWCNT nanocomposite on the photocatalytic degradation of cyanide (experimental conditions: light source, 150 W blue fluorescent lamp; reaction time, 30 min; dosage of photocatalyst, 1.6 g/L; volume of aqueous solution, 100 mL; and cyanide concentration, 100 mg/L).

## 4. Conclusions

$BiFeO_3$, Ag/$BiFeO_3$, and Ag/$BiFeO_3$-MWCNT samples were prepared and used for cyanide degradation under visible light irradiation. The prepared nanoparticles were investigated by several techniques, such as TEM, XRD, UV-Vis spectra, BET surface area analysis, and PL spectra, to investigate their physical and chemical properties. The XRD results revealed that a Ag/$BiFeO_3$-MWCNT nanocomposite composed of $BiFeO_3$, Ag and a MWCNT was distributed. The TEM results revealed that Ag and $BiFeO_3$ were homogenously dispersed on the MWCNT surface. The results revealed that the BET surface area of the Ag/$BiFeO_3$-MWCNT nanocomposite had a higher surface area compared with that of $BiFeO_3$ nanoparticles. UV-Vis measurements showed that modification of $BiFeO_3$ nanoparticles with Ag and MWCNT enabled the absorption of light at a high wavelength. PL analysis showed the drastic reduction in the band gap of the $BiFeO_3$ nanoparticles upon their modification with Ag and MWCNT, which greatly enhanced their photocatalytic performance. The photocatalytic activity performances of $BiFeO_3$, Ag/$BiFeO_3$, and Ag/$BiFeO_3$-MWCNT were investigated for cyanide degradation under visible light irradiation, and the findings showed that the Ag/$BiFeO_3$-MWCNT nanocomposite had the highest performance compared with the other nanoparticles. The Ag/$BiFeO_3$-MWCNT nanocomposite has great photocatalytic stability, which allowed it to be used for cyanide degradation in aqueous solution five successive times without losing its efficiency.

## Acknowledgments

This project was funded by the Deanship of Scientific Research (DSR), King Abdulaziz University, Jeddah, under grant no. G-23-130-1439 for their DSR technical and financial support.

## References

[1] N. Dwivedi, C. Balomajumder, P. Mondal, Comparative investigation on the removal of cyanide from aqueous solution using two different bioadsorbents, Water Resour. Ind., 15 (2016) 28–40
[2] S.C. Chena, J.K. Liu The response to cyanide of cyanide-resistant *Klebsiella oxytoca* bacterial strain FEMS, Microbiol. Ecol., 175 (1999) 37–43.
[3] C.D. Hébert, NTP Technical Report on Toxicity Studies of Sodium Cyanide (CAS No. 143-33-9).
[4] R.R. Dash, A. Gaur, C. Balomajumder, Cyanide in industrial wastewaters and its removal: a review on biotreatment, J. Hazard. Mater., 163 (2009) 1–11.
[5] O.A.A. Eletta, O.A. Ajayi, O.O. Ogunleye, I.C. Akpan, Adsorption of cyanide from aqueous solution using calcinated eggshells: equilibrium and optimization studies, J. Environ. Chem. Eng., 4 (2016) 1367–1375.
[6] N. Singh, C. Balomajumder, Simultaneous removal of phenol and cyanide from aqueous solution by adsorption onto surface modified activated carbon prepared from coconut shell, J. Water Process Eng., 9 (2016) 233–245.
[7] J. Shen, H. Zhao, H. Cao, Y. Zhang, Y. Chen, Removal of total cyanide in coking wastewater during a coagulation process: significance of organic polymers, J. Environ. Sci., 26 (2014) 231–239.
[8] O. Alonso-González, F. Nava-Alonso, C. Jimenez-Velasco, A. Uribe-Salas, Copper cyanide removal by precipitation with quaternary ammonium salts, Miner. Eng., 42 (2013) 43–49.
[9] S. Tian, Y. Li, X. Zhao, Cyanide removal with a copper/active carbon fiber cathode via a combined oxidation of a Fenton-like reaction and in situ generated copper oxides at anode, Electrochim. Acta, 180 (2015) 746–755.
[10] A.R. Yeddou, S. Chergui, A. Chergui, F. Halet, A. Hamza, B. Nadjemi, A. Ould-Dris, J. Belkouch, Removal of cyanide in aqueous solution by oxidation with hydrogen peroxide in presence of copper-impregnated activated carbon, Miner. Eng., 24 (2011) 788–793.
[11] M. Hijosa-Valsero, R. Molina, H. Schikora, M. Müller, J.M. Bayona, Removal of cyanide from water by means of plasma discharge technology, Water Res., 47 (2013) 1701–1707.
[12] A. Pala, R.R. Politi, G. Kurşun, M. Erol, F. Bakal, G. Öner, E. Çelik, Photocatalytic degradation of cyanide in wastewater using new generated nano-thin film photocatalyst, Surf. Coat. Technol., 271 (2015) 207–216.
[13] E.S. Baeissa, Synthesis and characterization of sulfur-titanium dioxide nanocomposite for photocatalytic oxidation of cyanide using visible light irradiation, Chin. J. Catal., 36 (2015) 698–704.
[14] X. Zhao, J. Zhang, J. Qu, Photoelectrocatalytic Oxidation of Cu-cyanides and Cu-EDTA at $TiO_2$ nanotube electrode, Electrochim. Acta, 80 (2015) 129–137.
[15] K. Chiang, R. Amal, T. Tran, Photocatalytic oxidation of cyanide: kinetic and mechanistic studies, J. Mol. Catal. A, 193 (2003) 85–297.
[16] S.H. Kim, S.W. Lee, G.M. Lee, B.-T. Lee, S.-T. Yun, S.-O. Kim, Monitoring of $TiO_2$-catalytic UV-LED photo-oxidation of cyanide contained in mine wastewater and leachate, Chemosphere, 143 (2016) 106–114.
[17] J.H. Li, B.F. Yan, X.S. Shao, S.-S. Wanga, H.-Y. Tianb, Q.-Q. Zhanga, Influence of Ag/$TiO_2$ nanoparticle on the surface hydrophilicity and visible-light response activity of polyvinylidene fluoride membrane, Appl. Surf. Sci., 324 (2015) 82–89.
[18] A. Bumajdad, M. Madkour, Understanding the superior photocatalytic activity of noble metals modified titania under UV and visible light irradiation, Phys. Chem. Chem. Phys., 16 (2014) 7146–7158.
[19] K.Y. Foo, B.H. Hameed, Decontamination of textile wastewater via $TiO_2$/activated carbon composite materials, Adv. Colloid Interface Sci., 159 (2010) 130–143.
[20] E.B. Simsek, Solvothermal synthesized boron doped $TiO_2$ catalysts: photocatalytic degradation of endocrine disrupting compounds and pharmaceuticals under visible light irradiation, Appl. Catal. B, 200 (2017) 309–322.

[21] R.M. Mohamed, E.S. Baeissa, Preparation and characterization of Pd–$TiO_2$–hydroxyapatite nanoparticles for the photocatalytic degradation of cyanide under visible light, Appl. Catal. A, 464–465 (2013) 218–224.
[22] Z. Mesgari, M. Gharagozlou, A. Khosravi, K. Gharanjig, Synthesis, characterization and evaluation of efficiency of new hybrid Pc/Fe-$TiO_2$ nanocomposite as photocatalyst for decolorization of methyl orange using visible light irradiation, Appl. Catal. A, 411–412 (2012) 139–145.
[23] F. Gao, X. Chen, K. Yin, S. Dong, Z. Ren, F. Yuan, T. Yu, Z. Zou, J.M. Liu, Visible light photocatalytic properties of weak magnetic $BiFeO_3$ nanoparticles, Adv. Mater., 19 (2007) 2889–2892.
[24] T. Gao, Z. Chen, Y. Zhu, F. Niu, Q. Huang, L. Qin, X. Sun, Y. Huang, Synthesis of $BiFeO_3$ nanoparticles for the visible-light induced photocatalytic property, Mater. Res. Bull., 59 (2014) 6–12.
[25] S. Li, Y.H. Lin, B.P. Zhang, Y. Wang, C.W. Nan, Controlled fabrication of $BiFeO_3$ uniform microcrystals and their magnetic and photocatalytic behaviors, J. Phys. Chem. C, 114 (2010) 2903–2908.
[26] S. Li, J. Zhang, M.G. Kibria, Z. Mi, M. Chaker, D. Ma, R. Nechache, F. Rosei, Remarkably enhanced photocatalytic activity of laser ablated Au nanoparticle decorated $BiFeO_3$ nanowires under visible-light, Chem. Commun. (Cambridge), 49 (2013) 5856–5858.
[27] S.M. Selbach, M.-A. Einarsrud, T. Tybell, T. Grande, Synthesis of $BiFeO_3$ by wet chemical methods, J. Am. Ceram. Soc., 90 (2007) 3430–3434.
[28] T. Fan, C. Chen, Z. Tang, Y. Ni, C. Lu, Synthesis and characterization of g-$C_3N_4$/$BiFeO_3$ composites with an enhanced visible light photocatalytic activity, Mater. Sci. Semicond. Process., 40 (2015) 439–445.
[29] F. Niu, D. Chen, L. Qin, N. Zhang, J. Wang, Z. Chen, Y. Huang, Facile synthesis of highly efficient p-n heterojunction CuO/$BiFeO_3$ composite photocatalysts with enhanced visible-light photocatalytic activity, ChemCatChem, 7 (2015) 3279–3289.
[30] K. Nakata, A. Fujishima, $TiO_2$ photocatalysis: design and applications, J. Photochem. Photobiol. C: Photochem. Rev., 13 (2012) 169–189.
[31] L.K. Pan, X.J. Liu, Z. Sun, C.Q. Sun, Nanophotocatalysts via microwave-assisted solution-phase synthesis for efficient photocatalysis, J. Mater. Chem. A, 1 (2013) 8299–8326.
[32] S.H. Han, K.S. Kim, H.G. Kim, H.G. Lee, H.W. Kang, J.S. Kim, C.I. Cheon, Synthesis and characterization of multiferroic $BiFeO_3$ powders fabricated by hydrothermal method, Ceram. Int., 36 (2010) 1365–1372.
[33] G.V. Subba Rao, C.N.R. Rao, Infrared and electronic spectra of rare earth perovskites: ortho-chromites, -manganites and -ferrites, Appl. Spectrosc., 24 (1970) 436–445.
[34] M. Yoon, M. Seo, C. Jeong, J.H. Jang, K.S. Jeon, Synthesis of liposome-templated titania nanodisks: optical properties and photocatalytic activities, Chem. Mater., 17 (2005) 6069–6079.
[35] V. Fruth, L. Mitoseriu, D. Berger, A. Ianculescu, C. Matei, S. Preda, M. Zaharescu, Preparation and characterization of $BiFeO_3$ ceramics, Prog. Solid State Chem., 35 (2007) 193–202.
[36] X. Wang, Y. Zhang, Z. Wu, Magnetic and optical properties of multiferroic bismuth ferrite nanoparticles by tartaric acid-assisted sol–gel strategy, Mater. Lett., 64 (2010) 486–488.
[37] D.A. Chang, P. Lin, T.Y. Tseng, Optical properties of $ZrTiO_4$ films grown by radio-frequency magnetron sputtering, J. Appl. Phys., 77 (1995) 4445–4451.
[38] Y.N. Huo, Y. Jin, Y. Zhang, Citric acid assisted solvothermal synthesis of $BiFeO_3$ microspheres with high visible-light photocatalytic activity, J. Mol. Catal. A: Chem., 331 (2010) 15–20.
[39] R.Q. Guo, L. Fang, W. Dong, F. Zheng, M. Shen, Enhanced photocatalytic activity and ferromagnetism in Gd doped $BiFeO_3$ nanoparticles, J. Phys. Chem. C, 114 (2010) 21390–21396.
[40] K.S. Suslick, S.B. Choe, A.A. Cichowlas, M.W. Grinstaff, Sonochemical synthesis of amorphous Iron, Nature, 353 (1991) 414–416.
[41] L. Zhou, W. Wang, L. Zhang, Ultrasonic-assisted synthesis of visible-light induced $Bi_2MO_6$ (M =W, Mo) photocatalysts, J. Mol. Catal. A: Chem., 268 (2007) 195–200.
[42] J. Lishan, D. Tong, L. Qingbiao, T. Yong, Study of photocatalytic performance of $SrFeO_3$ by ultrasonic radiation, Catal. Commun., 8 (2007) 963–966.
[43] D. Wang, J. Tang, Z. Zou, J. Ye, Photophysical and photocatalytic properties of a new series of visible-light-driven photocatalysts $M_3V_2O_8$ (M = Mg, Ni, Zn), Chem. Mater., 17 (2005) 5177–5182.
[44] J.G. Yu, J.F. Xiong, B. Cheng, S.W. Liu, Fabrication and characterization of Ag–$TiO_2$ multiphase nanocomposite thin films with enhanced photocatalytic activity, Appl. Catal. B, 60 (2005) 211–221.
[45] A.V. Deshpande, U. Kumar, Effect of method of preparation on photophysical properties of RhB impregnated sol–gel hosts, J. Non-Cryst. Solids, 306 (2002) 149–159.
[46] A. Ghanadzadeh, M.A. Zanjanchi, R. Tirbandpay, The role of host environment on the aggregative properties of some ionic dye materials, J. Mol. Struct., 616 (2002) 167–174.
[47] I. Lopez Arbeloa, P. Ruiz Ojeda, Dimeric states of Rhodamine B, Chem. Phys. Lett., 87 (1982) 556–560.
[48] S. Iijima, Helical Microtubules of Graphitic Carbon, Nature, 354 (1991) 56–58.
[49] T.A. Saleh, M.A. Gondal, Q.A. Drmosh, Z.H. Yamani, A. Al-Yamani, Enhancement in photocatalytic activity for acetaldehyde removal by embedding ZnO nanoparticles on multiwall carbon nanotubes, Chem. Eng. J., 166 (2011) 407–412.
[50] X.J. Wang, S.W. Yao, X.B. Li, Sol-gel preparation of CNT/ZnO nanocomposite and its photocatalytic property, Chin. J. Chem., 27 (2009) 1317–1320.
[51] L.P. Zhu, G.H. Liao, W.Y. Huang, L.L. Ma, Y. Yang, Y. Yu, S.Y. Fu, Preparation, characterization and photocatalytic properties of ZnO-coated multi-walled carbon nanotubes, Mater. Sci. Eng. B, 163 (2009) 194–198.
[52] R.M. Mohamed, M. Abdel Salam, Photocatalytic reduction of aqueous mercury(II) using multi-walled carbon nanotubes/Pd-ZnO nanocomposite, Mater. Res. Bull., 50 (2014) 85–90.
[53] T.A. Saleh, The Role of Carbon Nanotubes in Enhancement of Photocatalysis, syntheses and Applications of Carbon Nanotubes and Their Composites (book edit by S. Suzuki), InTech Publisher, Vol. 21, 2013, pp. 493–497.